Electrochimica Acta 177 (2015) 310–320

Contents lists available at ScienceDirect

Electrochimica Acta

journal homepage: www.elsevier.com/locate/electacta

Numerical analysis of vanadium crossover effects in all-vanadium redox flow batteries

Seongyeon Won, Kyeongmin Oh, Hyunchul Ju *

Department of Mechanical Engineering, Inha University, 100 Inha-ro, Nam-Gu Incheon 402-751, Republic of Korea

ARTICLE INFO

Article history:
Received 25 January 2015
Accepted 27 January 2015
Available online 29 January 2015

Keywords:
Numerical simulation
Vanadium redox flow battery
Vanadium ion crossover

ABSTRACT

In this work, a crossover model is newly developed to account rigorously for the crossover of vanadium ions through the membrane and resultant side reactions occurring in both positive and negative electrodes. The crossover model is then numerically coupled with previously developed three-dimensional (3-D), transient, thermal VRFB model in which key physicochemical phenomena including the electrochemical reactions, waste heat generation, resultant species and heat transport are all included. Using the comprehensive VRFB model, we investigate the effects of vanadium crossover between the negative and positive electrodes during a single charge/discharge cycle. Numerical simulations successfully capture capacity loss related to vanadium crossover, clearly showing the difference in species distributions due to side reactions. The results show that due to effect of vanadium ion crossover, more charging time and less discharging time have been achieved.

1. INTRODUCTION

All-vanadium redox flow batteries (VRFBs) utilize the V^{2+}/V^{3+} and VO_2^+/VO^{2+} redox couples in sulfuric acid as the anolyte and catholyte, respectively. Using the same vanadium species with the different oxidation states in both electrodes significantly mitigates the major critical issues in RFB technologies such as electrolyte cross-contamination, irreversible capacity loss, and undesirable side reactions. As a result, VRFBs exhibit relatively higher energy efficiency (up to 80%) and longer life-cycle among the redox flow batteries developed to date, showing the greatest commercial prospects for large-scale energy storage applications.

However, considerable crossover of vanadium ions and resultant capacity loss during charging and discharging processes have been continuously reported in the literature [1–3]. The fact implies that periodical electrolyte rebalancing and system maintenance are inevitably required for long-term VRFB operations, which in turn significantly raises operational cost of VRFB systems. Therefore, suppressing vanadium ions crossover must be one of key factors to achieve success in VRFBs and their widespread use.

The amount of vanadium crossover is mainly determined by ion-exchange membranes. So far, the commercial perfluorinated Nafion® membranes have been commonly used for VRFBs due to their high proton conductivity and excellent mechanical and chemical stability [4–7]. However, these membranes suffer from high cost and more importantly, high vanadium ions permeability. Therefore, considerable efforts have been made in the development of alternative ion-exchange membranes to meet the majority of aforementioned membrane characteristics for VRFBs [8–10].

Besides the development of new VRFB membranes, many groups have studied transport phenomena of vanadium ions through the membranes with a primary goal to obtain vanadium ions crossover data and analyze detailed crossover processes under different types of membranes and operating conditions [11–13]. Wiedemann et al. [14] measured the crossover diffusivity of vanadium ions through three different kinds of cation exchange membranes, i.e. CMX, CMS, and CMV membranes. They concluded that the CMS membrane is most suitable for VRFB applications due to its relatively lower crossover diffusivity values of vanadium ions ranging between 10^{-13} and 10^{-14} m^2/s. Sun et al. [15] experimentally analyzed vanadium ions crossover through Nafion 115 membrane, emphasizing that a major driving force for vanadium ions crossover is the concentration difference of vanadium ions between the positive and negative electrodes. In addition, their crossover data qualitatively showed the close interactions between vanadium ions, water, and proton transfer under various self-discharge and charge-discharge processes. Most recently, Lawton et al. [16] experimentally illustrated decreasing behavior of the permeation rate of VO^{2+} through Nafion 117 with increasing sulfuric acid concentration in the electrolyte solutions. They suspected the trend to be mainly caused by increasing level of

* Corresponding author. Tel.: +82 32 860 7312; fax: +82 32 868 1716.
E-mail address: hcju@inha.ac.kr (H. Ju).

http://dx.doi.org/10.1016/j.electacta.2015.01.166
0013-4686/

Nomenclature

A	cross-sectional area, m^{-2}
a	effective catalyst area per unit electrode volume, m^{-1}
C	molar concentration, mol m^{-3}
C_{KC}	Kozeny-Carman constant
D	diffusion coefficient, $m^2 s^{-1}$
E_0	thermodynamic equilibrium potential, V
F	Faraday's constant, 96,487 C mol^{-1}
h	heat transfer coefficient, W K^{-1}
I	current, A
j	transfer current density, A m^{-3}
K	effective permeability, m^2
k	reaction rate/coefficient, m s^{-1}, and thermal conductivity, W m^{-1} K^{-1}
M	molecular weight, kg mol^{-1}
$\vec{N}$	species flux, mol m^{-3} s^{-1}
P	pressure, Pa
Q	volumetric flow rate, $m^3 s^{-1}$
R	universal gas constant, 8.314 J mol^{-1} K^{-1}
r_p	pore radius, m
S	source/sink term
s	entropy, J K^{-1} mol^{-1}
T	temperature, K
$\vec{u}$	fluid velocity, m s^{-1}
V	volume, m^3
v	velocity, m s^{-1}
vf_i	volume fraction of species i

Greek symbols

α	transfer coefficient
ε	porosity
η	overpotential, V
κ	ionic conductivity, S cm^{-1}
μ	dynamic viscosity, kg m^{-1} s^{-1}
ρ	density, kg m^{-3}
σ	electronic conductivity, S cm^{-1}
τ	viscous shear stress, N m^{-2}
Φ	potential, V

Subscript

0	equilibrium or initial value
amb	ambient
cc	current collector domain
ch	charged species
dis	discharged species
elec	electrode
i	species index
in	channel inlet
l	liquid electrolyte domain
mem	membrane domain
NE	negative electrode
out	channel outlet
PE	positive electrode
s	solid electrode domain

Superscript

0	equilibrium or initial value
e	bulk electrolyte
eff	effective value
s	electrode surface
xover	crossover

membrane dehydration and resultant stronger partitioning/clustering effects with more sulfuric acid.

The issues of vanadium ions crossover have been also investigated by theoretical modeling and simulations. Skyllas-Kazacos and co-workers [17,18] presented simplified mathematical models wherein the mass and energy balance equations were coupled to describe the diffusion of vanadium ions through the membrane and predict resultant side reactions and capacity loss. However, electrochemical kinetics and the transport of charges were neglected in their models. Recently, Knehr et al. [19] accounted for all three crossover mechanisms of vanadium ions (i.e. diffusion, convection, and migration) in their two-dimensional (2-D), isothermal VRFB model. They numerically compared the relative magnitudes of diffusive, convective, and migrated fluxes and evaluated their contributions to total crossover flux during charging and discharging processes.

Although the aforementioned complex crossover phenomena entail a detailed account of electrolyte potential redistribution, various side reactions, and capacity loss, the crossover influences and related mechanisms were not precisely analyzed in the previous model development and theoretical analysis. In this paper, the above-mentioned crossover phenomena in VRFBs are newly modeled and incorporated into a 3-D electrochemical-transport-thermal coupled model for VRFBs. In this model, we consider four different oxidation states of vanadium ions, bisulfate, proton, and water as crossover species and account for relevant side reactions due to these crossover species in the negative and positive electrodes of VRFBs. In addition, the three crossover mechanisms including diffusion, convection, and migration are taken into account in order to more accurately capture the effects of crossover phenomena during VRFB operations. The 3-D simulation results presented in this study clearly address detailed crossover impacts on multi-dimensional species distributions as well as on overall thermal-electrochemical behaviors of VRFBs and capacity loss during charging/discharging cycles.

2. Model development

The model considers essential parts of the VRFBs including membrane, porous carbon electrodes and current collectors for a single cell. The schematic diagram and computational domain used for the simulation is well displayed on Figs. 1 and 2.

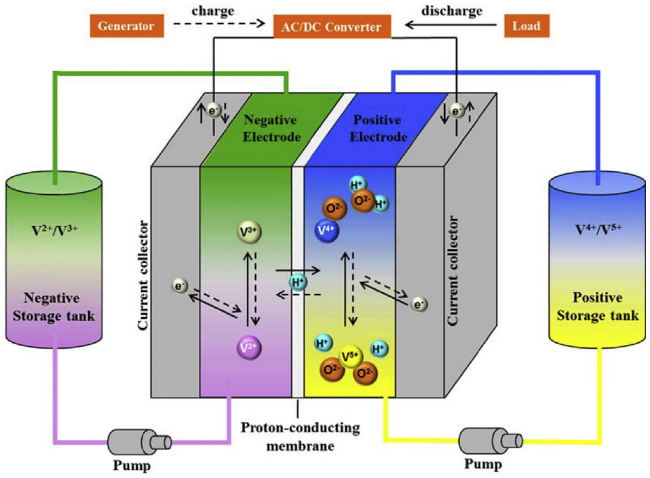

Fig. 1. Schematic diagram of VRFB illustrating the redox reactions and transport processes.

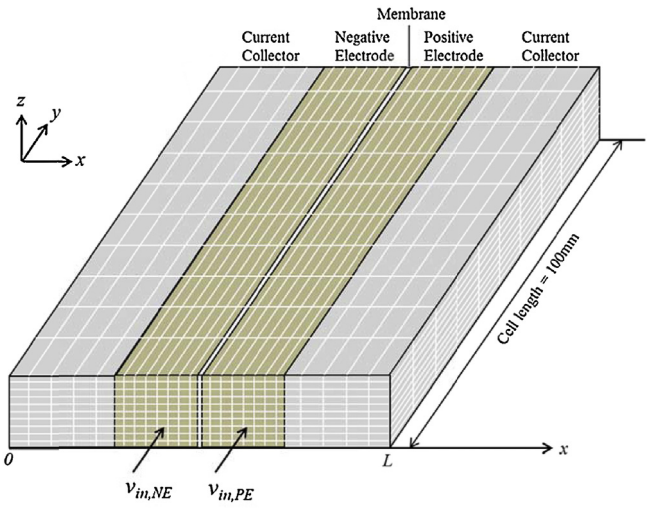

Fig. 2. Computational domain and mesh configuration of a simple VRFB geometry.

2.1. Model assumptions

For the simulation of VRFB, the practical conditions hard to deal with should be idealized as follows even it includes some errors:

1. The electrolyte flow is incompressible and laminar due to the small pressure gradient and low flow velocity.
2. The gas bubble formation caused by the side reactions in the electrodes are ignored.
3. The dilute-solution approximation is used for describing the species transport phenomena.
4. Water permeation or drag through the membrane is ignored.
5. The characteristics of the electrode, electrolyte and membrane are assumed to be isotropic.

2.2. Conservation equations and source terms

The five conservation equations (mass, momentum, species, charge, and thermal energy) are applied to each components of VRFBs (Table 1). First, The mass and momentum conservation equations applied to the electrodes and membrane domain are given as follows:

Mass conservation:

$$\frac{\partial \varepsilon \rho}{\partial t} + \nabla \cdot (\rho \vec{u}) = 0 \tag{1}$$

Momentum conservation:

$$\frac{1}{\varepsilon}\left[\frac{\partial \rho \vec{u}}{\partial t} + \frac{1}{\varepsilon}\nabla \cdot (\rho \vec{u}\vec{u})\right] = -\nabla P + \nabla \cdot \tau + \rho \vec{g} + S_u \tag{2}$$

where ε denotes the porosity of the porous carbon electrodes and superficial velocities are used in above equations for the mass flux continuity at the interface between the porous and nonporous regions inside a VRFBs. Also, ρ is volume-averaged density of all liquid species considered in the model and is calculated by the following equation.

$$\rho = \sum_i \rho_i \cdot vf_i = \sum_i C_i \cdot M_i \tag{3}$$

In Eq. (3),vf_i is volume fraction of species i in the liquid electrolyte. In addition, C_i and M_i represent molar concentration and molecular weight of species i in the mixture, respectively. S_u in the right hand side of Eq. (2) is the momentum source term used to closely consider the restricted condition of the porous carbon electrodes in which the permeability is small and thus the velocity is small. The Darcy's law is employed with the Kozeny-Carman equation in order to satisfy the above-mentioned conditions:

$$S_u = -\left(\frac{\mu}{K}\right)\vec{u} \tag{4}$$

$$K = \frac{4r_p^2 \quad \varepsilon^3}{C_{KC}(1-\varepsilon)^2} \tag{5}$$

K in Eq. (5) denotes the effective permeability of the porous carbon electrodes and corresponding Kozeny-Carman constant, C_{KC} is shown in Table 2.

The species in the model (i.e. water, proton and vanadium ions) are governed by three transport mechanisms including diffusion, convection, and migration. For describing the three modes of transport phenomena of each species in the porous electrodes and membrane, the species conservation equation is used as follows:

Species conservation:

$$\frac{\partial(\varepsilon C_i)}{\partial t} + \nabla \cdot \vec{N}_i = S_i \tag{6}$$

As to the calculation for the transport of sulfuric acid, HSO_4^-, it is not included in the above equation for the liquid electrolyte is assumed to be electroneutral.

$$\sum_i z_i C_i = 0 \tag{7}$$

where z_i is the valence of species i.

The term S_i in right hand side of Eq. (6) is for the description of production/dissolution of each species i caused by redox reaction during the charge and discharge processes and are clearly displayed in Table 1. In addition, $\vec{N}_i$ represents species fluxes by means of convection, diffusion, and migration which are formulated by the Nernst-Planck equation:

$$\vec{N}_i = \vec{u}C_i - D_i^{eff}\nabla C_i - \frac{z_i F D_i^{eff} C_i}{RT}\nabla \Phi_e \tag{8}$$

Table 1
VRFB model: source/sink terms.

Term	Positive electrode		Negative electrode	
S_i	VO^{2+}	$-\frac{j_{PE}}{F} + 3\frac{n_{V^{2+}}^{xover}}{\delta_{PE}} + 2\frac{n_{V^{3+}}^{xover}}{\delta_{PE}}$	V^{2+}	$\frac{j_{NE}}{F} - \frac{n_{VO^{2+}}^{xover}}{\delta_{NE}} - 2\frac{n_{VO_2^+}^{xover}}{\delta_{NE}}$
	VO_2^+	$\frac{j_{PE}}{F} - 2\frac{n_{V^{2+}}^{xover}}{\delta_{PE}} - \frac{n_{V^{3+}}^{xover}}{\delta_{PE}}$	V^{3+}	$-\frac{j_{NE}}{F} + 2\frac{n_{VO^{2+}}^{xover}}{\delta_{NE}} + 3\frac{n_{VO_2^+}^{xover}}{\delta_{NE}}$
	H^+	$2\frac{j_{PE}}{F} - 2\frac{n_{V^{2+}}^{xover}}{\delta_{PE}}$	H^+	$-2\frac{n_{VO^{2+}}^{xover}}{\delta_{NE}} - 4\frac{n_{VO_2^+}^{xover}}{\delta_{NE}}$
S_Φ	Φ_s	$-j_{PE}$	Φ_s	$- j_{NE}$
	Φ_e	j_{PE}	Φ_e	j_{NE}
S_T	Q_{act}	$\eta_{PE} j_{PE}$	Q_{act}	$\eta_{NE} j_{NE}$
	Q_{rev}	$j_{PE} T\frac{dU_0}{dT}\vert_{PE}$	Q_{rev}	$-j_{NE} T\frac{dU_0}{dT}\vert_{NE}$
	Q_{ohm}	$\frac{I_e^2}{\kappa^{eff}} + \frac{I_s^2}{\sigma^{eff}}$	Q_{ohm}	$\frac{I_e^2}{\kappa^{eff}} + \frac{I_s^2}{\sigma^{eff}}$
	Membrane		Current Collector	
	Q_{act}	0	Q_{act}	0
	Q_{rev}	0	Q_{rev}	0
	Q_{ohm}	$\frac{I_e^2}{\kappa_{mem}}$	Q_{ohm}	$\frac{I_s^2}{\sigma_{cc}}$

Table 2
Kinetic, physiochemical, and transport properties.

Symbol	Description	Value	Ref.
D_{H^+}	H^+ diffusivity in electrode	$9.3\times10^{-9}\,m^2\,s^{-1}$	[20]
$D_{VO^{2+}}$	VO^{2+} diffusivity in electrode	$3.9\times10^{-10}\,m^2\,s^{-1}$	[22]
$D_{VO_2^+}$	VO_2^+ diffusivity in electrode	$3.9\times10^{-10}\,m^2\,s^{-1}$	[22]
$D_{V^{2+}}$	V^{2+} diffusivity in electrode	$2.4\times10^{-10}\,m^2\,s^{-1}$	[22]
$D_{V^{3+}}$	V^{3+} diffusivity in electrode	$2.4\times10^{-10}\,m^2\,s^{-1}$	[22]
$D_{H^+,mem}$	H^+ diffusivity in membrane	$3.35\times10^{-9}\,m^2\,s^{-1}$	[22]
$D_{VO^{2+}}^{xover}$	Crossover diffusivity of VO^{2+}	$5.0\times10^{-12}\,m^2\,s^{-1}$	[19]
$D_{VO_2^+}^{xover}$	Crossover diffusivity of VO_2^+	$1.17\times10^{-12}\,m^2\,s^{-1}$	[19]
$D_{V^{2+}}^{xover}$	Crossover diffusivity of V^{2+}	$3.125\times10^{-12}\,m^2\,s^{-1}$	[19]
$D_{V^{3+}}^{xover}$	Crossover diffusivity of V^{3+}	$5.93\times10^{-12}\,m^2\,s^{-1}$	[19]
σ_s	Electronic conductivity of electrode	$500\,S\,m^{-1}$	[22]
σ_{cc}	Electronic conductivity of current collector	$1000\,S\,m^{-1}$	[22]
r_p	Pore radius of electrode	$1.0\times10^{-5}\,m$	[22]
C_{KC}	Kozeny-Carman constant: porous electrode	5.55	[22]
k_{PE}	Rate constant in positive electrode	$2.5\times10^{-8}\,m\,s^{-1}$	[19]
k_{NE}	Rate constant in negative electrode	$7.0\times10^{-8}\,m\,s^{-1}$	[19]
a	Effective catalyst area/unit electrode volume	$3.5\times10^{4}\,m^{-1}$	[19]
α_{PE}	Transfer coefficient in positive electrode	0.55	[19]
α_{NE}	Transfer coefficient in negative electrode	0.45	[19]

At the right hand side of above equation, the first term denotes the convection flux of each species wherein $\vec{u}$ is velocity vector of the electrolyte in the porous electrodes. And the second and third terms represent diffusion and migration fluxes, respectively, and D_i^{eff} in these terms means effective diffusion coefficient of ionic species i, modified by using the Bruggeman correlation [21] to consider the effects of porosity and tortuosity in the porous electrodes:

$$D_i^{eff} = \varepsilon^{3/2} D_i \tag{9}$$

Electrons and charged ions are generated/vanished due to the electrochemical reactions in the electrodes and move in the opposite direction which is governed by the principle of conservation of charge:

$$\nabla\cdot\vec{i}_e = -\nabla\cdot\vec{i}_s = j \tag{10}$$

where j is transfer current density caused by vanadium redox reactions and $\vec{i}_e$ denotes the ionic current density through the various VRFB components.

$$\vec{i}_e = F\sum_i z_i\vec{N}_i = \sum_i\left(z_iF\vec{u}C_i - z_iFD_i^{eff}\nabla C_i - \frac{z_i^2F^2D_i^{eff}C_i}{RT}\nabla\Phi_e\right) \tag{11}$$

In regard to the third term in the right hand side of Eq. (11), the effective ionic conductivity of the electrolyte, κ^{eff}, for the electrode and membrane regions can be defined as follows:

$$\kappa^{eff} = \frac{F^2}{RT}\sum_i z_i^2 D_i^{eff} C_i \tag{12}$$

In addition, $\vec{i}_s$ in Eq. (10) means electronic current density through the electrodes and current collectors.

$$\vec{i}_s = \sigma^{eff}\nabla\Phi_s \tag{13}$$

The electronic conductivity, σ^{eff}, should be differently applied to the porous electrodes and current collectors; for the electrodes are porous region, the Bruggeman correlation [21] is adopted as follows:

$$\sigma^{eff} = \begin{cases} (1-\varepsilon)^{3/2}\sigma_s & \text{Porous electrodes} \\ \sigma_{cc} & \text{Current colletors} \end{cases} \tag{14}$$

The electrochemical reactions accompany various types of heat generation which is well considered by following energy conservation equation:

$$\frac{\partial\overline{\rho c_p}T}{\partial t} + \nabla\cdot\left((\rho c_p)_l\vec{u}T\right) = \nabla\cdot\left(k^{eff}\nabla T\right) + S_T \tag{15}$$

Table 3
Thermal properties of VRFB [23].

Symbol	Description	Value
k_l	Thermal conductivity of electrolyte	$0.67\,W\,m^{-1}\,K^{-1}$
k_s	Thermal conductivity of solid electrode	$0.15\,W\,m^{-1}\,K^{-1}$
k_{mem}	Thermal conductivity of membrane	$0.67\,W\,m^{-1}\,K^{-1}$
k_{cc}	Thermal conductivity of current collector	$16\,W\,m^{-1}\,K^{-1}$
$(\rho c_p)_l$	Thermal capacitance of electrolyte	$4.19\times10^{6}\,J\,m^{-3}\,K^{-1}$
$(\rho c_p)_s$	Thermal capacitance of solid electrode	$3.33\times10^{5}\,J\,m^{-3}\,K^{-1}$
$\rho_{mem}c_{p,mem}$	Thermal capacitance of membrane	$2.18\times10^{6}\,J\,m^{-3}\,K^{-1}$
$\rho_{cc}c_{p,cc}$	Thermal capacitance of current collector	$4.03\times10^{6}\,J\,m^{-3}\,K^{-1}$
h	Heat transfer coefficient	$2.57\,W\,K^{-1}$
Δs_{NE}	Entropy change associated with reaction in Eq. (1)	$-100\,J\,mol^{-1}\,K^{-1}$
Δs_{PE}	Entropy change associated with reaction in Eq. (2)	$-21.7\,J\,mol^{-1}\,K^{-1}$

In the above equation, the overall heat capacity, $\overline{\rho c_p}$, and effective thermal conductivity, k^{eff} are defined for various VRFB components:

$$\overline{\rho c_p} = \begin{cases} \varepsilon(\rho c_p)_l + (1-\varepsilon)(\rho c_p)_s & \text{Porous electrodes} \\ \rho_{mem} C_{p,mem} & \text{Membrane} \\ \rho_{cc} C_{p,cc} & \text{Current collectors} \end{cases} \quad (16)$$

$$k^{eff} = \begin{cases} \varepsilon k_l + (1-\varepsilon) k_s & \text{Porous electrodes} \\ k_{mem} & \text{Membrane} \\ k_{cc} & \text{Current collectors} \end{cases} \quad (17)$$

where $\overline{\rho c_p}$ and k^{eff} for the porous electrodes are attained by integrating the properties of liquid electrolytes (subscript "l") and solid electrodes (subscript "s"). The values for thermal properties of each components of VRFB are listed in Table 3. Also, the energy source term, S_T, in Eq. (15) is for describing the irreversible heat of the redox reactions, entropic heat, and Joule heating which can be seen in Table 1 for several VRFB components.

2.3. Electrochemical reactions in the porous electrodes

During the charge and discharge stages, the redox reactions of vanadium species take place simultaneously in the porous electrodes.

Negative electrode:

$$V^{3+} + e^- \rightleftarrows^{charge}_{discharge} V^{2+} \quad E_{0,NE} = -0.255V \text{ vs. SHE} \quad (18)$$

Positive electrode:

$$VO^{2+} + H_2O \rightleftarrows^{charge}_{discharge} VO_2^+ + e^- + 2H^+ \quad E_{0,PE} = 1.004V \text{ vs. SHE} \quad (19)$$

In the above equations, $E_{0,NE}$ and $E_{0,PE}$ denote the standard equilibrium potentials, respectively, and are obtained from thermodynamic properties under standard state conditions. Additionally, the transfer current density, j in Eq. (10) can be expressed by the Butler-Volmer equations as follows:

For the negative electrode:

$$j = aFk_{NE}\left(\frac{C^e_{V^{2+}}}{C^e_{V^{3+}}}\right)^{1-2\alpha_{NE}} \times \left[C^s_{V^{2+}}\exp\left(\frac{(1-\alpha_{NE})F\eta_{NE}}{RT}\right) - C^s_{V^{3+}}\exp\left(\frac{-\alpha_{NE}F\eta_{NE}}{RT}\right)\right] \quad (20)$$

For the positive electrode:

$$j = aFk_{PE}\left(\frac{C^e_{VO^{2+}}}{C^e_{VO_2^+}}\right)^{1-2\alpha_{PE}} \times \left[C^s_{VO^{2+}}\exp\left(\frac{(1-\alpha_{PE})F\eta_{PE}}{RT}\right) - C^s_{VO_2^+}\exp\left(\frac{-\alpha_{PE}F\eta_{PE}}{RT}\right)\right] \quad (21)$$

The values of reaction rate constant, k, the effective catalyst area per unit electrode volume, a, and the charge transfer coefficient, α are presented in Table 2. Furthermore, C_i^e indicates the bulk concentration of vanadium ion i in the liquid electrolyte within the porous electrodes and C_i^s denotes the surface concentration of vanadium ion i on the interfacial surface between solid electrode and liquid electrolyte which is calculated by following equations [19,22]:

For the charged species ($C_{ch} = C_{V^{2+}}$ or $C_{VO_2^+}$):

$$C^s_{ch} = C^e_{ch} - \frac{r_p}{D_{ch}}k(C^e_{ch})^{1-2\alpha}(C^e_{dis})^{-(1-2\alpha)} \times \left[C^s_{ch}\exp\left(\frac{(1-\alpha)F\eta}{RT}\right) - C^s_{dis}\exp\left(\frac{-\alpha F\eta}{RT}\right)\right] \quad (22)$$

For the discharged species ($C_{dis} = C_{V^{3+}}$ or $C_{VO^{2+}}$):

$$C^s_{dis} = C^e_{dis} - \frac{r_p}{D_{dis}}k(C^e_{ch})^{1-2\alpha}(C^e_{dis})^{-(1-2\alpha)} \times \left[C^s_{dis}\exp\left(\frac{-\alpha F\eta}{RT}\right) - C^s_{ch}\exp\left(\frac{(1-\alpha)F\eta}{RT}\right)\right] \quad (23)$$

In addition, the overpotential, η for the negative and positive electrodes are as follows:

$$\eta_{NE} = \Phi_s - \Phi_e - E_{NE} \quad (24)$$

$$\eta_{PE} = \Phi_s - \Phi_e - E_{PE} \quad (25)$$

where Φ_s and Φ_e are the electronic potential in the solid electrodes and ionic potential in the liquid electrolyte, respectively. Also, E_{NE} and E_{PE} are the equilibrium potentials of the negative and positive electrodes, respectively, and are derived from the standard equilibrium potential which takes into account the effect of temperature change during the VRFB operation.

$$E_{NE} = E_{0,NE} + \frac{dE_0}{dT}|_{NE}(T - T_0) \quad (26)$$

$$E_{PE} = E_{0,PE} + \frac{dE_0}{dT}|_{PE}(T - T_0) \quad (27)$$

The terms related to the temperature difference, $dE_0/dT|_i$ in Eqs. (26) and (27), can be expressed as a function of entropy change during electrochemical reactions as follows:

$$\frac{dE_0}{dT}|_i = \frac{\Delta s_i}{nF} \quad (28)$$

The entropy changes corresponding with the negative and positive electrodes are shown in Table 3.

2.4. Vanadium ions crossover model and relevant source terms

In order to account for the crossover of vanadium ions through the membrane, the crossover model is newly developed and incorporated into a comprehensive VRFB model described in Sections 2.1 to 2.3. Once the vanadium ions in the negative electrode, V^{2+}, V^{3+} transport across the membrane, the following side reactions can occur in the positive electrode;

$$V^{2+} + 2VO_2^+ + 2H^+ \rightarrow 3VO^{2+} + H_2O \quad (29)$$

$$V^{3+} + VO_2^+ \rightarrow 2VO^{2+} \quad (30)$$

On the other hand, the crossover of VO^{2+} and VO_2^+ from the positive to negative electrodes results in the following side reactions in the negative electrode, i.e.

$$VO^{2+} + V^{2+} + 2H^+ \rightarrow 2V^{3+} + H_2O \quad (31)$$

$$VO_2^+ + 2V^{2+} + 4H^+ \rightarrow 3V^{3+} + 2H_2O \quad (32)$$

Therefore, it is evident that the crossover of vanadium ions through the membrane and resultant side reactions causes an imbalance in vanadium ions between the negative and positive electrodes, which gives rise to loss of capacity. For monitoring the degree of capacity losses with the cycle number, the coulombic efficiency is defined as follows:

$$\text{Coulombic efficiency} = \frac{\text{discharge capacity}}{\text{charge capacity}} \times 100 = \frac{t_{dis}}{t_{ch}} \times 100 \quad (33)$$

The consequence of crossed-over vanadium ions appear in the source terms of the species equation. Table 1 shows the additional source terms due to the crossover and resultant side reactions wherein n_i^{xover} denotes the crossover molar flux of species, i across the membrane, i.e. calculated based on the Nernst-Planck equation in Eq. (8). Here, the assumption has been made that the crossed-over vanadium ions from one electrode are uniformly consumed throughout the other electrode.

2.5. Species and energy balance equations

The vanadium species in the electrolyte tanks come into the porous electrodes and depart the VRFB cell as seen in the computational domain (Fig. 2). During the charging/discharging processes, the redox reactions occur in the porous electrodes which makes the concentrations of vanadium ions and the electrolyte temperature change with time. For electrolyte flows continuously, the species and thermal management of VRFB is automatically handled as following equations:

$$\frac{\partial C_i^{\text{tank}}}{\partial t} = \frac{Q_{\text{pump}}}{V_{\text{tank}}}\left(C_{i,out}^{VRFB} - C_{i,in}^{VRFB}\right) \quad (34)$$

$$\frac{\partial T^{\text{tank}}}{\partial t} = \frac{Q_{\text{pump}}}{V_{\text{tank}}}\left(T_{out}^{VRFB} - T_{in}^{VRFB}\right) \quad (35)$$

In the above equations, for the VRFB simulation, the outlet concentration and temperature of electrolyte are assumed to be the states of anolyte/catholyte tanks and then directly used to the inlet data for the next time step.

2.6. Initial/boundary conditions and model implementation

The inlet velocities, v_{in} of electrolyte entering the porous electrodes are calculated by using the volumetric flow rate, Q, driven by pumps on which magnitude of that are same for the anolyte and catholyte.

$$v_{in} = \frac{Q_{pump}}{\varepsilon A} \quad (36)$$

where A is inlet area of either electrodes. Also, no-slip and impermeable velocity conditions are applied to the external surfaces of electrodes apart from the inlets and outlets. With regard to thermal boundary condition, the top and bottom surfaces of the computational domain is treated as adiabatic and the convective boundary condition is applied to the left and right edges of current collectors of the domain to the purpose of single cell approximation [23]:

$$-k^{eff}\frac{\partial T}{\partial \vec{n}} = h(T - T_{amb}) \quad (37)$$

where $\vec{n}$ and T_{amb} are the unit normal vector out of the current collectors and ambient temperature, respectively.

For the simulation is performed under galvanostatic operation, the constant current density is applied to the right and left side walls of current collectors during the charge and discharge processes.

$$-\sigma_{cc}\nabla\Phi_s \cdot \vec{n} = \begin{cases} -\dfrac{I}{A_{cc}} (x = 0) \\ \dfrac{I}{A_{cc}} (x = L) \end{cases} \quad (38)$$

I in above equation is current applied to the cell. And the sign convention is based on the charging stage so that it should be reversed during the discharge process. But for the side walls of the cell, the front, rear, top and bottom surfaces are assumed to be electrically insulated.

Table 4
Cell geometric and operating conditions for VRFB simulations.

Description	Value
Electrode length	0.1 m
Electrode height	0.004 m
Thickness of membrane	180×10^{-6} m
Thickness of current collector	0.006 m
Volume of electrolyte tank, V_{tank}	0.00125 L
Initial temperature	25 °C
Initial V^{2+} concentration	110.7 mol m^{-3}
Initial V^{3+} concentration	996.3 mol m^{-3}
Initial VO^{2+} concentration	996.3 mol m^{-3}
Initial VO_2^+ concentration	110.7 mol m^{-3}
Initial H^+ concentration	5000 mol m^{-3}
Volumetric flow rate, Q_{pump}	0.001 L s^{-1}
Applied current density	0.1 A cm^{-2}

The cell geometric and initial/operating conditions for VRFB simulation are listed in Table 4. Also, kinetic, physiochemical and transport properties, and thermal properties are displayed in Tables 2 and 3, respectively. The aforementioned VRFB model was implemented in the commercial fluid dynamics (CFD) software program, Fluent, by using user-defined functions (UDFs). The convergence criteria were set to 10^{-6} for the equation residuals. The grid and time-step sizes are inversely related to the spatial and temporal gradients of the variables calculated by the VRFB simulations; these parameters were prudently selected based on the transient fuel cell simulation results of the present group and sensitivity studies performed by other VRFB modeling groups [24–28]. The number of grid points required to sufficiently resolve the spatial gradients in the computational domain is 3600 (i.e., approximately $36 \times 10 \times 10$ in the x, y, and z directions, respectively). On the other hand, the maximum time-step size required to ensure adequate time resolution for the VRFB simulations is 0.5 s.

3. RESULTS AND DISCUSSION

To examine the effects of vanadium crossover, two different membranes representing fresh and degraded membranes were taken into consideration for VRFB simulations. The fresh membrane is defined based on the vanadium ion permeability measured by Jingyu Xi et al. [29] and from that data, E.C. Kumbur et al. calculated the crossover diffusivities of vanadium ions [19] (i.e. listed in Table 2). In the literature, it has been reported that major outcomes of membrane degradation are membrane decomposition and pinhole formation, which results in higher permeation rates of the reactant fluid [30]. Therefore, the crossover diffusivities were raised by one order of magnitude to approximate degraded membrane. It should be noted that for each parametric case, the uniform crossover rate is applied to the entire membrane area, which represents that the membrane is degraded uniformly.

Fig. 3 displays the cell voltage and SOC curves during a single charge and discharge cycle. During the charging process, the longer charge time is required with the degraded membrane ($10 \times D_i^{xover}$) due to the stronger vanadium crossover and resultant side reactions; the charge times to reach the SOC of 0.85 for the fresh and degraded membrane cases are 2130.5 s and 2201 s, respectively. Contrarily, the discharge time becomes shorter from 2060.5 s to 1996.5 s due to the membrane

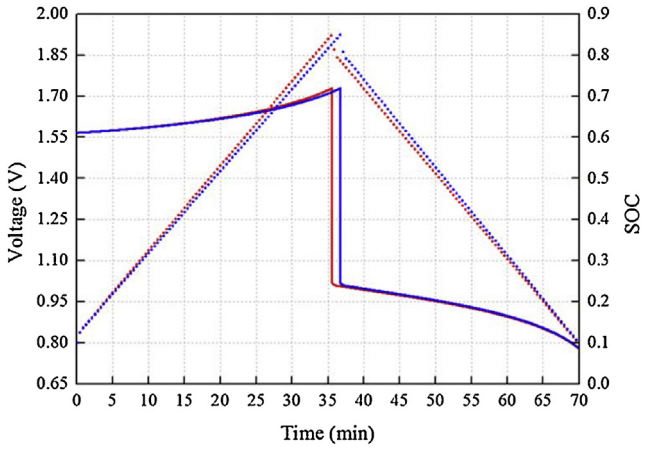

Membrane	Fresh	Degraded
Charging time	35m 30.5s	36m 41s
Discharging time	34m 20.5s	33m 16.5s
Coulombic efficiency	96.714%	90.709%

Fig. 3. Comparison of cell performance and SOC evolution curves during a single VRFB charging and discharging cycle with the fresh and degraded membranes. The vanadium crossover diffusivities in the degraded membrane were assumed to be 10 times larger than those of fresh membrane.

degradation. As a result, the coulometric efficiency, i.e. defined in Eq. (33) with the degraded membrane is 90.709% during the single charge/discharge cycle, i.e. 6% lower than that of the fresh membrane (96.714%). The numerical comparison between the fresh and degraded membranes clearly addresses that the capacity loss can be significantly accelerated as the membrane is degraded.

The total vanadium concentrations in the negative and positive electrodes are plotted in Fig. 4 during the charge and discharge processes. Regardless of the degree of membrane degradation, the same trend is observed in the evolution of vanadium concentrations; the vanadium concentration in the negative electrode ($V^{2+} + V^{3+}$) increases during charge and then decreases during discharge whereas the vanadium concentration in the positive electrode ($VO^{2+} + VO_2^+$) exhibits the opposite trend, decreasing and increasing behaviors during the charge and discharge processes, respectively. These trends are indicative of considerable influences of migration and subsequent side reactions on overall vanadium crossover through the membrane. During charge, the migration flux is directed from the positive to negative electrodes, which results in an increase in the overall vanadium concentration ($V^{2+} + V^{3+}$) in the negative electrode and reduction in the vanadium concentration in the positive electrode ($VO^{2+} + VO_2^+$). Conversely, the direction of migration is reversed during discharge, being toward the positive electrode. Therefore, the opposite behaviors of vanadium concentrations in the negative and positive electrodes are observed during discharge.

More importantly, a comparison of vanadium concentrations between the fresh and degraded membrane cases clearly indicates that the capacity loss becomes severer with the higher vanadium crossover diffusivities in the degraded membrane. During charge, the total amount of vanadium in the negative electrode ($V^{2+} + V^{3+}$) more steeply increase with the degraded membrane while more substantial drop in $VO^{2+} + VO_2^+$ is observed with the membrane. On the other hand, during discharge, the quicker decrease in the overall concentration of $V^{2+} + V^{3+}$ in the negative electrode and

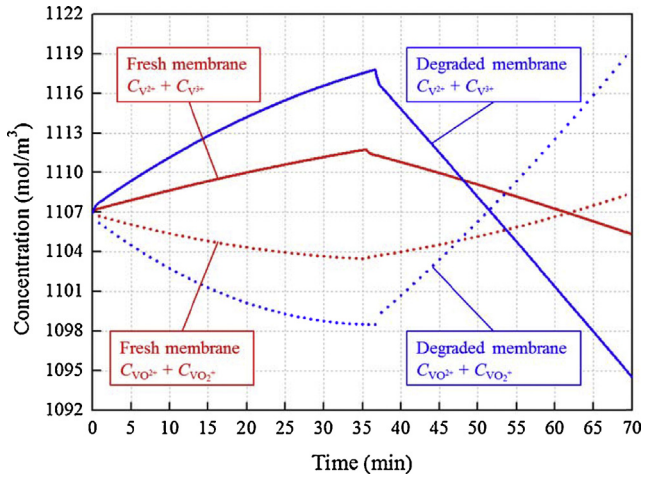

Fig. 4. Evolution of vanadium concentrations in the negative and positive electrodes during a single charging and discharging cycle with 0.1 A/cm^2 under different levels of membrane degradation.

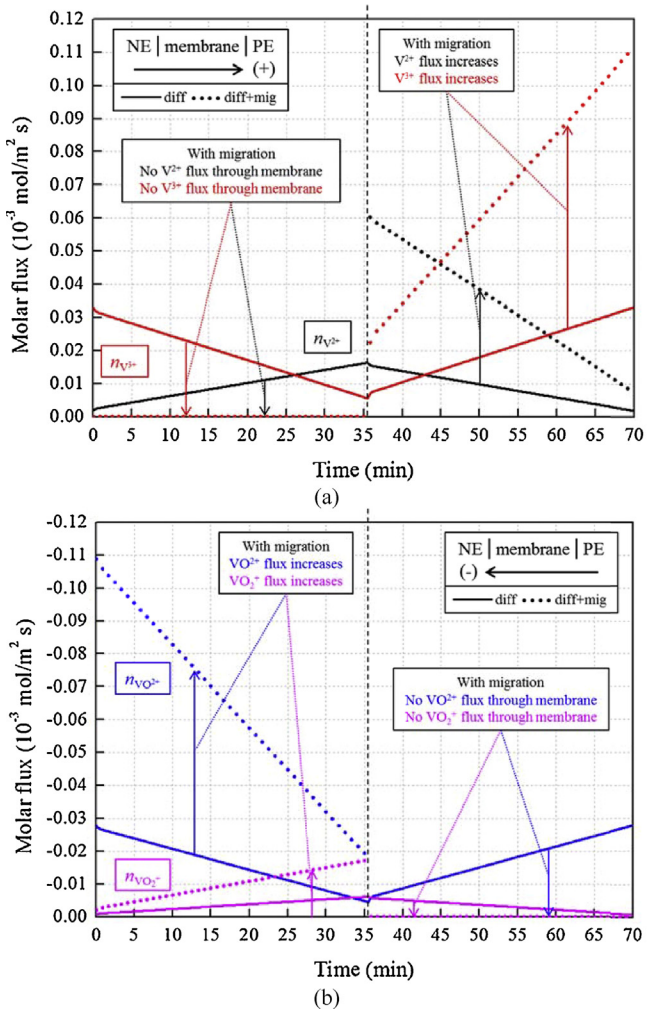

Fig. 5. Crossover fluxes of vanadium species through the membrane during a single charging and discharging cycle with 0.1 A/cm^2 with the fresh membrane (1xD^{xover}): (a) negative electrode species (V^{2+} and V^{3+}); (b) positive electrode species (VO^{2+} and VO_2^+).

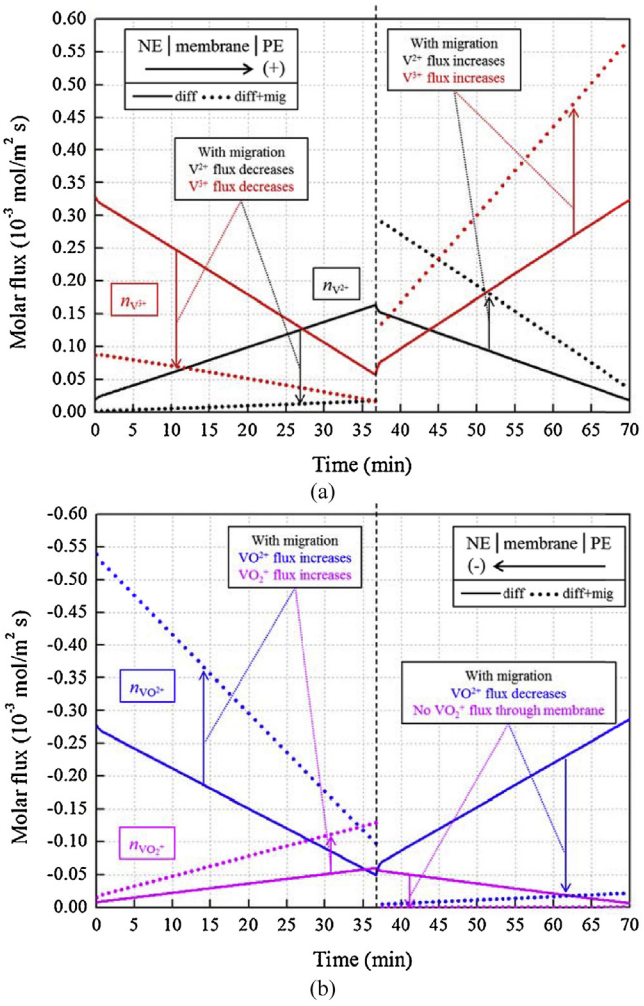

Fig. 6. Crossover fluxes of vanadium species through the membrane during a single charging and discharging cycle with 0.1 A/cm^2 with the degraded membrane (10xD^{xover}): (a) negative electrode species (V^{2+} and V^{3+}); (b) positive electrode species (VO^{2+} and VO_2^+).

faster increase in the overall concentration of $VO^{2+} + VO_2^+$ in the positive electrode were predicted in the degraded membrane case. For more detailed analysis, the vanadium crossover fluxes for the fresh and degraded membrane cases are plotted in Figs. 5 and 6, respectively. In these plots, a positive value represents vanadium crossover from the negative electrode to the positive electrode. In addition, 'diff' denotes the vanadium crossover flux driven by diffusion only whereas 'diff+mig' represents the total flux of vanadium species driven by both diffusion and migration. It is seen in Fig. 5 (the fresh membrane case) that although the diffusive fluxes of vanadium species in the negative electrode (V^{2+} and V^{3+}) are positive during charge, the total fluxes of V^{2+} and V^{3+} are zero, implying that there is no net flux toward the positive electrode. That is indicative of considerable migration fluxes from the positive electrode to the negative electrode. Consequently, as seen in Fig. 4, the total amount of vanadium in the negative electrode ($V^{2+} + V^{3+}$) with the fresh membrane increases during charge. On the other hand, for the degraded membrane case shown in Fig. 6, the overall concentrations of V^{2+} and V^{3+} in the negative electrode are positive during charge, implying that the negative electrode loses V^{2+} and V^{3+} to the positive electrode. That indicates the strong diffusion fluxes through the degraded membrane. Nevertheless, as seen in Fig. 4, the total amount of vanadium in the negative electrode ($V^{2+} + V^{3+}$) in the degraded membrane case even more steeply increases during charge. The trend is because the crossover of VO^{2+} and VO_2^+ from the positive electrode to negative electrode is substantial in the degraded membrane and subsequently the significant amount of V^{3+} is produced in the negative electrode via the side reactions of Eqs. (29) and (30). In Fig. 4, very high values of V^{3+} concentration in the degraded membrane case during charge is clearly indicative of vigorous crossover of VO^{2+} and VO_2^+ and side reactions.

As above-mentioned, the vanadium diffusion across the membrane has a significant influence on the capacity loss during VRFB operations, which further illustrates that the choice of a suitable membrane is critical, giving a significant impact on establishing an operating strategy of VRFBs to minimize the capacity loss. Fig. 7 shows the evolution of SOC and the total amount of vanadium species in the negative and positive electrodes under three different thicknesses of membrane. It is observed that the magnitude of capacity loss, i.e. proportional to the discrepancy of vanadium concentrations between the negative and positive electrodes. During charging, the total vanadium ion concentration in negative electrode ($V^{2+} + V^{3+}$) increases more with thicker membrane, whereas that in positive electrode ($VO^{2+} + VO_2^+$) decreases. However, these trends are completely reversed during discharging and

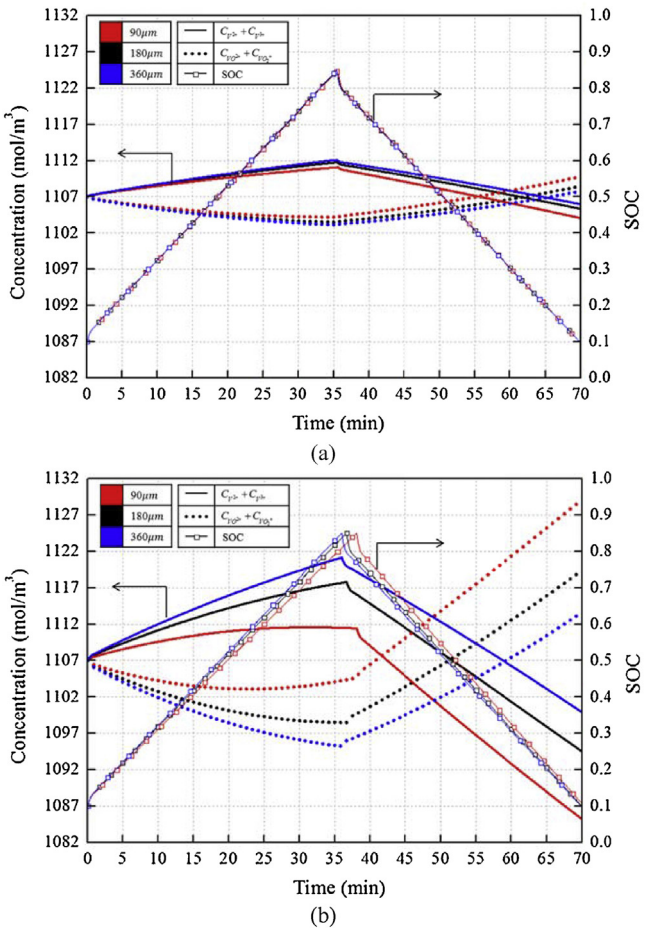

Fig. 7. Evolution of SOC and overall amount of vanadium species in the negative and positive electrodes during a single charge/discharge cycle under different membrane thicknesses for (a) fresh membrane and (b) degraded membrane. The current density for charge and discharge is 0.1 A/cm^2.

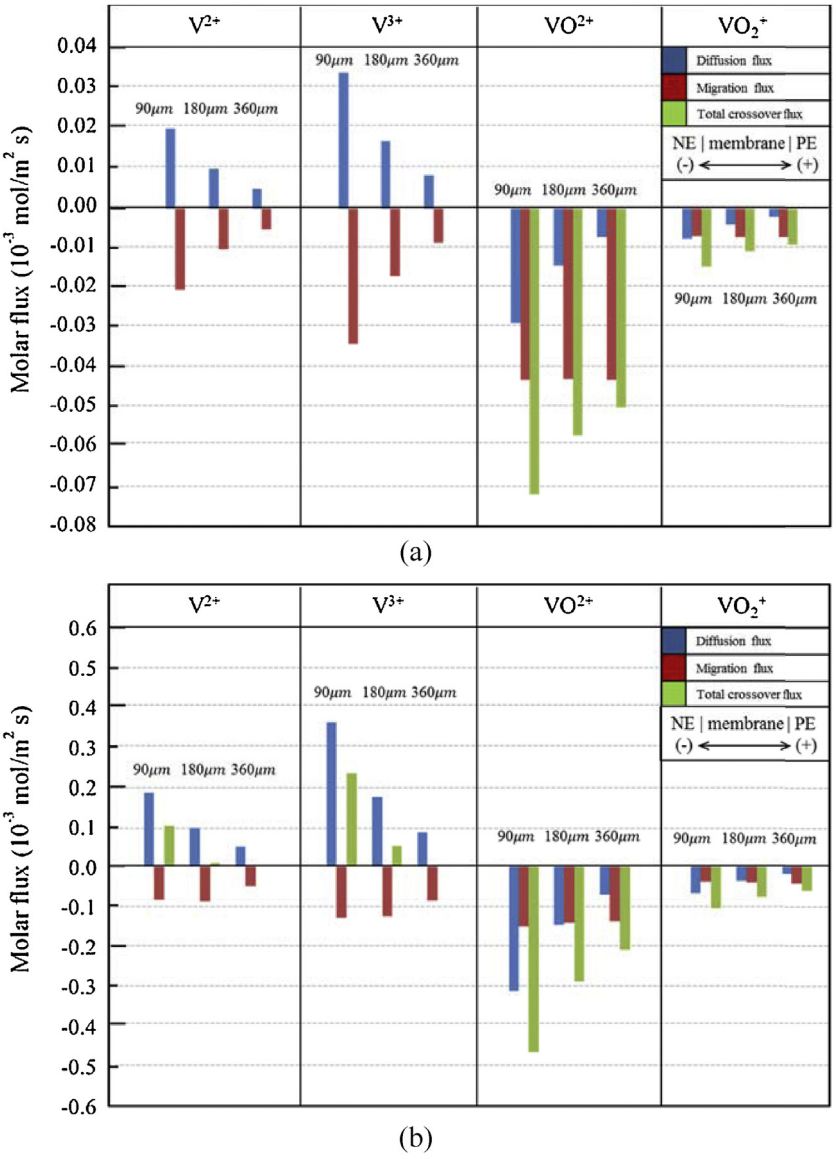

Fig. 8. Average crossover fluxes through the membrane comprising diffusion and migration fluxes under different membrane thickness after 20 min of the beginning of charging process for (a) fresh membrane and (b) degraded membrane.

consequently, positive electrode concentration becomes higher than the negative electrode one. In addition, the difference is getting higher along with the degradation of membrane, which results in significant concentration imbalance between electrodes and consequent capacity loss for the thinner membrane. In order to explain these trends, the average crossover fluxes through the membrane after 20 min after the beginning of charging and discharging process are shown in Figs. 8 and 9 respectively. In Fig. 8(a), Due to the migration flux from membrane to electrode cannot exceed the diffusion one, the diffusion and migration fluxes are totally same from negative electrode to positive electrode for three different fresh membranes. On the other hand, the fluxes from positive to negative electrode are intensified by the migration fluxes, and then the fluxes are solely towards from positive to negative electrode, which means the increase of negative electrode species by the side reactions. For the degraded membrane in Fig. 8(b), compared to the fluxes from negative to positive electrode, the opposite directional fluxes are much higher causing the significant concentration difference between electrodes as described above. The diffusion crossover fluxes through the membrane are higher because the thinner membrane means the shorter crossover pathway to the other electrode. However, for the diffusion crossover fluxes increase in both electrodes, the net vanadium species crossover is smaller with the thinner membrane, and hence the concentration imbalance between electrodes is mitigated. During discharging process, as shown in Fig. 9, the diffusion fluxes increases with thinner membrane, but the net crossover flux of vanadium species from negative to positive electrode is similar for each membrane thickness, which means the increase of vanadium species crossover in negative electrode is similar with that in positive electrode. Therefore, the concentration imbalance between electrodes in Fig. 7 are derived by the higher net crossover flux during charging process.

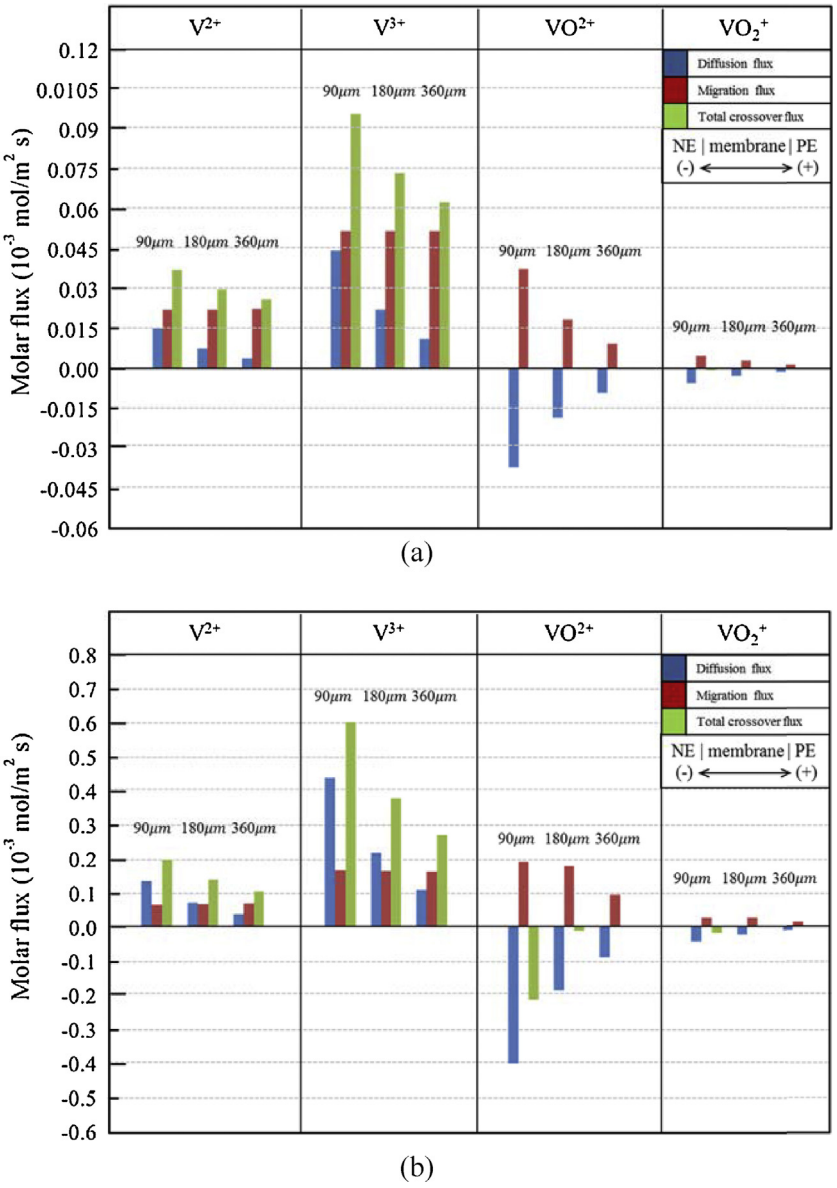

Fig. 9. Average crossover fluxes through the membrane comprising diffusion and migration fluxes under different membrane thickness after 20 min of the beginning of discharging process for (a) fresh membrane and (b) degraded membrane.

4. CONCLUSION

In this paper, the analysis of the effect of vanadium ion crossover through the membrane and resultant capacity losses was presented using 3-D transient VRFB model developed in our previous work. The purpose of this study is to numerically investigate the effect of vanadium ion crossover on VRFB performance. The model accounts for the diffusion and migration crossover through the membrane and relative side reactions in each electrode.

The simulation results show that the vanadium ion crossover has a negative effect on cell performance with degradation of the membrane, which was assumed to be 10 times higher crossover diffusivities of each vanadium ions through the membrane than those of the fresh membrane. The crossover effect became severe with degraded membrane and the coulombic efficiency is 6% lower than the fresh membrane. As the crossover and side reactions are continuously occurred in each electrode, the concentration between negative and positive electrode shows high imbalance: negative electrode concentration increases and positive one decreases during charging; the opposite trends were shown during discharging. In addition, the crossover fluxes show that the migration mitigates the crossover flux of negative electrode species during charging and intensifies that of positive electrode species, and moreover, the degradation of membrane enlarges the imbalance between electrodes.

Furthermore, to investigate the effect of the length of crossover path, the simulations with different membrane thickness were conducted. It is shown that the thinner membrane is applied, the higher diffusion crossover fluxes were calculated whereas the migration fluxes were remained same level. However, with degraded membrane, the increase of diffusion flux in thinner membrane mitigates the net crossover from positive to negative electrode during charging. Hence, the concentration imbalance is smaller compared to that of other membrane thickness. During discharging, the net crossover flux from negative to positive electrode is similar for all the membrane thicknesses, and finally, the concentration imbalance is large with the thinner membrane.

This paper contributes to enhancing the basic understanding of vanadium ion crossover through the membrane and relative side reactions during charging and discharging cycle of VRFB operation. This crossover model can act as a valuable tool for finding the optimum operating strategy of VRFBs in order to minimize the crossover through the membrane and resultant capacity loss.

ACKNOWLEDGEMENT

This work was supported by INHA UNIVERSITY Research Grant. We also thank to the TAESUNG S&E, INC. Korea for lending technical support towards ANSYS-FLUENT software.

References

[1] C. Sun, J. Chen, H. Zhang, X. Han, Q. Luo, Investigations on transfer of water and vanadium ions across Nafion membrane in an operating vanadium redox flow battery, J. Power Sources 195 (2010) 890–897.
[2] Q. Luo, H. Zhang, J. Chen, P. Qian, Y. Zhai, Modification of Nafion membrane using interfacial polymerization for vanadium redox flow battery applications, J. Mem. Sci. 211 (2008) 98–103.
[3] S. Kim, J. Yan, B. Schwenzer, J. Zhang, L. Li, J. Liu, Z. Yang, M.A. Hickner, Cycling performance and efficiency of sulfonated poly(sulfone) membranes in vanadium redox flow batteries, Elec. Comm. 12 (2010) 1650–1653.
[4] M. Skyllas-Kazacos, D. Kasherman, D.R. Hong, M. Kazacos, Characteristics and performance of 1kW UNSW vanadium redox battery, J. Power Sources 35 (1991) 399–404.
[5] X. Luo, Z. Lu, J. Xi, Z. Wu, W. Zhu, L. Chen, X. Qiu, Influences of Permeation of Vanadium Ions through PVDF-g-PSSA Membranes on Performances of Vanadium Redox Flow Batteries, J. Phys. Chem. B 109 (2005) 20310–20314.
[6] H. Prifti, A. Parasuraman, S. Winardi, T.M. Lim, M. Skyllas-Kazacos, Membranes for Redox Flow Battery Applications, Membranes 2 (2012) 275–306.
[7] Q. Luo, H. Zhang, J. Chen, P. Qian, Y. Zhai, Modification of Nafion membrane using interfacial polymerization for vanadium redox flow battery applications, J. Mem. Sci. 311 (2008) 98–103.
[8] T. Mohammadi, M. Skyllas-Kazacos, Characterisation of novel composite membrane for redox flow battery application, J. Mem. Sci. 98 (1995) 77–87.
[9] B. Tian, C.W. Yan, F.H. Wang, Modification and evaluation of membranes for vanadium redox battery applications, J. Applied Electrochemistry 34 (2004) 1205–1210.
[10] T. Mohammadi, M. Skyllas-Kazacos, Preparation of sulfonated composite membrane for vanadium redox flow battery applications, J. Mem. Sci 107 (1995) 35–45.
[11] T. Mohammadi, M. Skyllas-Kazacos, Evaluation of the chemical stability of some membranes in vanadium solution, J. Appled Electrochemistry 27 (1997) 153–160.
[12] J. Xi, Z. Wu, X. Qiu, L. Chen, Nafion/SiO_2 hybrid membrane for vanadium redox flow battery, J. Power Sources 166 (2007) 531–536.
[13] J. Xi, Z. Wu, X. Teng, Y. Zhao, L. Chen, X. Qiu, Self-assembled polyelectrolyte multilayer modified Nafion membrane with suppressed vanadium ion crossover for vanadium redox flow batteries, J. Materials Chemistry 18 (2008) 1232–1238.
[14] E. Wiedemann, A. Heintz, R.N. Lichtenthaler, Transport properties of vanadium ions in cation exchange membranes: Determination of diffusion coefficients using a dialysis cell, J. Mem. Sci 141 (1998) 215–221.
[15] C. Sun, J. Chen, H. Zhang, X. Han, Q. Luo, Investigations on transfer of water and vanadium ions across Nafion membrane in an operating vanadium redox flow battery, J. Power Sources 195 (2010) 890–897.
[16] J.S. Lawton, A. Jones, T. Zawodzinski, Concentration dependence of VO^{2+} crossover of Nafion for vanadium redox flow batteries, J. Elec. Soc. 160 (2013) A697–A702.
[17] A. Tang, J. Bao, M. Skyllas-Kazacos, Dynamic modelling of the effects of ion diffusion and side reactions on the capacity for vanadium redox flow battery, J. Power Sources 196 (2011) 10737–10747.
[18] A. Tang, J. Bao, M. Skyllas-Kazacos, Thermal modelling of battery configuration and self-discharge reactions in vanadium redox flow battery, J. Power sources 216 (2012) 489–501.
[19] K.W. Knehr, E. Agar, C.R. Dennison, A.R. Kalidindi, E.C. Kumbur, A transient vanadium flow battery model incorporating vanadium crossover and water transport through the membrane, J. Elec. Soc. 159 (2012) A1446–A1459.
[20] D. You, H. Zhang, J. Chen, A simple model for the vanadium redox battery, Electrochim. Acta 54 (2009) 6827–6836.
[21] R.E. Meredith, C.W. Tobias, in: C.W. Tobias (Ed.), Advances in Electrochemistry and Electrochemical Engineering, vol. 2, Interscience Publishers, New York, 1962.
[22] A.A. Shah, M.J. Watt-Smith, F.C. Walsh, A dynamic performance model for redox-flow batteries involving soluble species, Electrochim. Acta 53 (2008) 8087–8100.
[23] H. Al-Fetlawi, A.A. Shah, F.C. Walsh, Non-isothermal modelling of the all-vanadium redox flow battery, Electrochim. Acta 55 (2009) 78–89.
[24] H. Al-Fetlawi, A.A. Shah, F.C. Walsh, Modelling the effects of oxygen evolution in the all-vanadium redox flow battery, Electrochim. Acta 55 (2010) 3192–3205.
[25] J. Ko, H. Ju, Comparison of numerical simulation results and experimental data during cold-start of polymer electrolyte fuel cells, Applied Energy 94 (2012) 364–374.
[26] J. Ko, H. Ju, Numerical evaluation of a dual-function microporous layer under subzero and normal operating temperatures for use in automotive fuel cells, Int. J. Hydrog. 39 (2014) 2854–2862.
[27] J. Ko, W. Kim, Y. Lim, H. Ju, Improving the cold-start capability of polymer electrolyte fuel cells (PEFCs) by using a dual-function micro-porous layer (MPL): Numerical simulations, Int. J. Hydrog. 38 (2013) 652–659.
[28] P. Chippar, H. Ju, Evaluating cold-start behaviors of end and intermediate cells in a polymer electrolyte fuel cell (PEFC) stack, Solid State Ionics 225 (2012) 85–91.
[29] J. Xi, Z. Wu, X. Teng, Y. Zhao, L. Chen, X. Qiu, Self-assembled polyelectrolyte multilayer modified Nafion membrane with suppressed vanadium ion crossover for vanadium redox flow batteries, J. Materials Chemistry 18 (2008) 1232–1238.
[30] H. Tang, S. Peikang, S.P. Jiang, F. Wang, M. Pan, A degradation study of Nafion proton exchange membrane of PEM fuel cells, J. power sources 170 (2007) 85–92.